Jurnal Ilmu Fisika
Vol. 18, No. 1, March 2026, pp. 35–44
ISSN: 1979-4657 (Print); 2614-7386 (Online)
https://doi.org/10.25077/jif.18.1.35-44.2026

Jurnal Ilmu Fisika
Open Access

Enhancing Stellar Orbit Accuracy through the Radius Power Law Time Step Function Model

Hasanuddin Hasanuddin, Agustinus Eusebius, Yudha Arman

Department of Physics, Faculty of Mathematics and Natural Sciences, University of Tanjungpura, Pontianak, 78124, Indonesia.

Article Info

Article History:

Received July 08, 2025
Revised September 21, 2025
Accepted October 04, 2025
Published online October 09, 2025

Keywords:

astrophysical systems
numerical integration
stellar orbits
symplectic integrator
time step function

Corresponding Author:

Hasanuddin Hasanuddin,
Email: hasanuddin@physics.untan.ac.id

ABSTRACT

Accurately determining stellar orbits within astrophysical systems is paramount for understanding celestial mechanics. This study proposes a novel approach to enhance orbit accuracy by incorporating a radius power law time step function model. The methodology involves the numerical integration of the system's dynamics using a forward fourth-order symplectic integrator, combined with a time step function dependent on the distance of the test particle from the system's center. We conduct simulations on various astrophysical scenarios represented by conservative potentials, including point mass, Plummer, and Hernquist models. Our results demonstrate that employing a power-law time step function with an exponent of 1.5 significantly reduces phase-space error (measured by the ratio of radial to orbital periods) and improves orbit accuracy (measured by the gradient of the relative total energy drift). The method is easy to implement, computationally efficient, and adaptable to N-body and more general dynamical systems. Its solid theoretical basis and numerical reliability make it a practical tool for improving orbit accuracy in diverse astrophysical applications.

1. INTRODUCTION

An astrophysical system encompasses many phenomena, from planetary systems to cosmology. One particularly intriguing aspect of these systems is the orbit of individual objects within them. For instance, this includes the orbit of a star around a globular cluster or, even more fascinatingly, the orbit of a globular cluster around a galaxy.

The study of astrophysical systems initially involved an N-body astrophysical problem, where N represents the number of objects within the system (Aarseth & Heggie, 1993; Aarseth, 2003; Heggie & Hut, 2003; Dehnen & Read, 2011). This problem consists of $6N$ differential equations, with $3N$ initial positions and $3N$ initial momenta provided. When N is greater than 2, it becomes necessary to solve these equations numerically. The complexity of the problem increases when the systems experience close encounters among individual constituents (or become collisional systems). Several authors have proposed enlightened algorithms to address this challenging problem (Hernandez & Dehnen, 2023).

In contrast, in collisionless astrophysical systems where close encounters do not occur, the problem simplifies to that of a test particle orbiting within a smooth potential (Binney & Tremaine, 2008). In such scenarios, orbit integration can be employed using the provided potential.

While the simplification of the problem has already been achieved, orbit integration remains prone to numerical errors. These errors stem from the integration method, such as opting for lower-order accuracy methods instead of higher-order ones or choosing less time-reversible and non-symplectic methods over their counterparts. Another source of numerical error is the choice of time step. When an integrator uses a constant time step in orbit integration, the phase error can be somewhat disruptive, although the energy error remains constant for a conservative potential. To address this issue, the time step is expressed as a function of one or several physical properties of the orbit, as previously done by several authors (Zemp et al., 2007; Dehnen & Read, 2011; Dehnen, 2017; Dehnen & Hernandez, 2017). Recently, Pham et al. (2024) proposed a time step dependent on mixed variables, such as position, velocity, acceleration, and subsequent time derivatives of acceleration, albeit at the expense of expensive computation regarding the total number of time derivative calculations (Pham et al., 2024). Hasanuddin (2020) employed a variable time step based on the position of the test particle in a harmonic oscillator potential and reduced the phase error by about 75% (Hasanuddin, 2020b).

The time step previously utilised by Hasanuddin (2020b) has inspired us to adopt a time step function that depends on the position of the test particle relative to the system's centre. While the earlier work applied this approach to a one-dimensional harmonic oscillator with a simple time step inversely proportional to radius, we extend it by exploring a more general power-law dependence and using it to stellar orbits instead. Specifically, we employ a simple power-law function to determine the variable time step in orbit integration within a conservative potential, in contrast to the mixed and numerous variables used by Pham et al. (2024). We aim to establish the most effective power-law function for the time step, reducing the mean phase error while maintaining a minimal gradient of energy error drift.

We conduct a straightforward test on a system comprising point mass objects, such as planets orbiting a stationary star. Subsequently, we extend this test to stars orbiting within globular clusters and dark matter. Additionally, we apply our method to particles orbiting well-known spherical conservative potentials, such as the Plummer potential (Plummer, 1911, 1915) and Hernquist potential (Hernquist, 1990; Baes & Dejonghe, 2002).

The paper is structured as follows. Section 2 outlines the methodology, discussing the concept of the time step function, algorithm, and simulation setup. Section 3 focuses on presenting the results and subsequent discussion. We begin with a simple test on orbit simulations within a point mass potential and then apply the method to systems governed by the Plummer and Hernquist potential. Finally, we conclude in Section 4. Additional computed quantities for orbit integration are provided in the appendix.

2. METHOD

We aim to numerically solve a system of 6*N* first-order ordinary differential equations given by,

$$\dot{w} = \frac{\partial w}{\partial x_i}\frac{\partial H}{\partial p_i} - \frac{\partial w}{\partial p_i}\frac{\partial H}{\partial x_i}, \tag{1}$$

where $w = \{x_i, p_i\}$ represents the phase space for $i = 1,2,3$ and H is the Hamiltonian of the conservative system (Leimkuhler & Reich, 2005; Dehnen & Read, 2011). Here, $\dot{w}$ denotes the time derivative of the phase space. Decomposing the phase space into position (r) and velocity (r). The resulting differential equations are:

$$\frac{dr}{dt} = v \tag{2}$$

and

$$\frac{dv}{dt} = -\nabla\phi \tag{3}$$

where r, v, and ϕ represent the system's position, velocity, and potential, respectively.

Given the initial position r_0 and initial velocity v_0, equations (2) and (3) can be numerically solved using a fourth-order symplectic integrator, such as the Chin-Chen method (Chin & Chen, 2005). In this integrator, the subsequent updated velocity and position are calculated as follows:

$$v_{1/6} = v_0 + \frac{1}{6} a_0 h, \tag{4}$$

$$r_{1/2} = r_0 + \frac{1}{2} v_{1/6} h, \tag{5}$$

$$v_{5/6} = v_{1/6} + \frac{4}{6}\left(a_{1/2} + \frac{1}{48} g_{1/2} h^2\right) h, \tag{6}$$

$$r_1 = r_{1/2} + \frac{1}{2} v_{5/6} h. \tag{7}$$

Here, the subscript in vectors refers to the fraction of the full time step h (Hands et al., 2019). For example, $v_{1/6}$ represents the velocity of the particle evaluated at 1/6 of a time step, $r_{1/2}$ represents the position of the test particle evaluated at 1/2 of a time step, and so on.

This method introduces an additional vector g. Which can be calculated as (Chin & Chen, 2005):

$$g = \nabla(\nabla\Phi)^2 \tag{8}$$

or, equivalently,

$$g = 2\nabla\Phi \cdot \nabla(\nabla\Phi), \tag{9}$$

where $\nabla\Phi$ and $\nabla(\nabla\Phi)$ represent the potential gradient and tidal force tensor, respectively. In equation (6), $g_{1/2}$ takes the form $2\nabla\Phi(r_{1/2}) \cdot \nabla\left(\nabla\Phi(r_{1/2})\right)$. We prefer to implement the equation (9) in our code rather than the equation (8), as the tidal force tensor information can be used for other purposes in the simulation. We list the form of potential gradient and tidal force tensor in Appendix A for the central potential and Appendices B, C, and D for the point mass, Plummer, and Hernquist potentials, respectively.

2.1 Time Step Function

We propose a time step function that depends on the distance of the test particle from the centre of the system, *r*, in the form of a power law:

$$h = \eta \left(\frac{r}{a}\right)^{\alpha}. \tag{10}$$

Here, $\eta, \alpha,$ and a represent the accuracy parameter, power, and scale radius, respectively. Since r may change over time, h may also vary, making h implicitly dependent on time. The scale radius, denoted by a, signifies the maximum radius the test particle can have. Since this maximum radius is unknown at the beginning, we define the constant scale radius as GM/E_0, where G is the universal gravitational constant, M is the total mass of the system, and E_0 is the initial total energy of the test particle.

The rationale behind employing such a time step is that as the test particle moves at higher speeds, the time step needs to decrease to uphold orbit accuracy. This relationship is based on the particle's speed being inversely proportional to its radius, as illustrated by Kepler's second law. Therefore, the time step may be correlated with the test particle's radius through a power-law model.

2.2 Algorithm

We initiate the process by providing the integrator equations (4) to (7), with the initial position and velocity, along with the time step computed according to the equation (10). Subsequently, we capture the updated position and velocity, utilising these values for the subsequent iteration and recording them to a file. This iterative process persists until the desired time is attained. These steps are represented by a flow chart in Figure 1.

In the simulation, we use a Python 3 module named Simpthon, which is publicly available (Hasanuddin, 2020a). This module employs an abstract base class for both potential and integrator. To initialise a specific potential (for example, a point mass potential), we can use the following code in the Python terminal:

```
>>> import simpthon as S
>>> pot = S.potential.pointmass(GM=1.)
```

Given the potential, we can set up an integrator as follows:

```
>>> itg = S.integrator.Forward4OSymplectic(pot)
```

We can later invoke the integrator to update the position and velocity of the particle. The integrator takes the time step as one of its parameters.

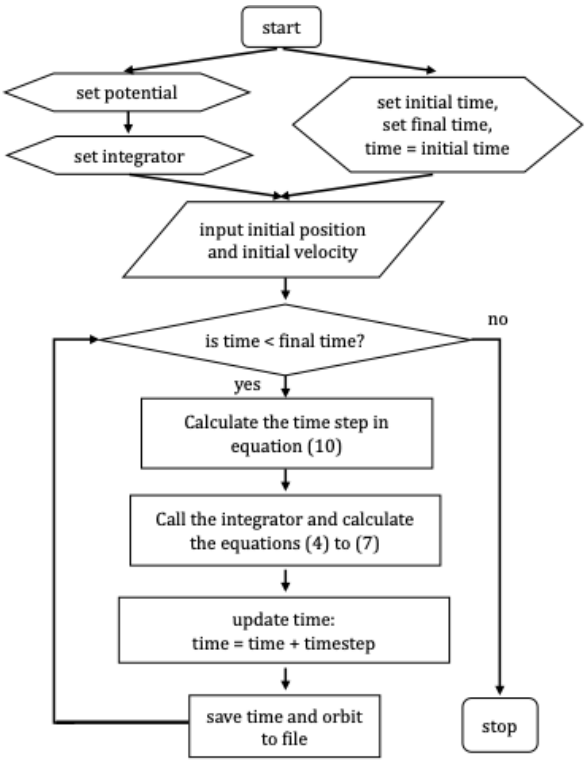

Figure 1. The flowchart of the simulation process.

After the simulation stops, we calculate the relative total energy error, ε, at each time step using the data from the saved file:

$$\varepsilon = \frac{E_t - E_0}{E_0}. \tag{11}$$

Here, E_0 and E_t represent the initial total energy and total energy at time t of the test particle, respectively. Additionally, we compute the ratio of the radial and orbital periods to demonstrate the precession of the orbit:

$$\frac{\Delta\theta}{2\pi} = \frac{T_r}{T_\theta}. \tag{12}$$

Theoretically, the radial and orbital periods of the test particle's orbit remain constant, thus resulting in a continuous precession of the orbit, and the phase error can be quantified.

2.3 Simulation Setup

In this simulation, Cartesian coordinates are employed, with the centre of the system located at the origin. The simulation commences with the test particle positioned at (1,0,0) and moving with a

velocity of (0,0.25,0), corresponding to a highly eccentric orbit (e>0.9). The constant GM is set to 1, allowing for the arbitrary selection of length units. Velocity units are established accordingly. For example, if we choose the mass of the centre of the system (M) in solar mass ($M_{\odot}$) and the unit length to be parsec (pc), the unit of velocity is approximately $65.58\sqrt{M}$ m/s or $1.02\sqrt{M} \times 10^3$ pc/Myr.

3. RESULTS AND DISCUSSION

We conducted multiple simulations until the test particle completed 100 orbits around the system's centre, adhering to the parameters established in the simulation setup. The outcomes of our simulations are as follows:

3.1 First Test on Point Mass Potential

Examples of point mass potentials include a system of a planet orbiting a star (such as a planet around the Sun) or a binary system where a two-body problem can be simplified. The point mass potential is represented by the simple potential equation:

$$\Phi(r) = -\frac{GM}{r}. \tag{13}$$

In this potential, orbits can be precisely determined and are characterised by conic sections. When the test particle is bound to the system, the orbit forms an ellipse with an eccentricity exceeding 0.9. We can validate the results of numerical integration by directly comparing the high eccentric orbits, as depicted in Figure 2. Using a high eccentric orbit in the numerical integration is a challenging method. Figure 2 shows that integration with a constant time step exhibits phase space errors, although the energy drift remains flat (Hasanuddin, 2022). In contrast, the exact orbit does not precess as observed in the integration with a time step following a power law of 1.5.

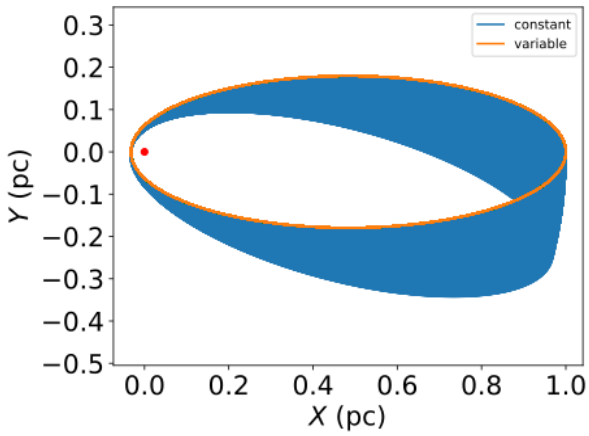

Figure 2. The orbit of a test particle in a point mass potential resulting from constant (blue line) and variable (orange line) time step ($\propto r^{3/2}$).

As the point mass potential is conservative, energy conservation is maintained. We can, therefore, assess our power law time step model by observing the energy drift across various values of the parameter α, as defined in the equation (10). Our findings indicate that the energy drift is linear for all α parameters. Moreover, this linear drift's gradient is minimised when set to 1.5, as depicted in Figure **3**.

Throughout one orbit, the energy error oscillates due to the radial oscillation of the orbit. Additionally, we quantify the phase space error across all parameter values of α by calculating the ratio of the radial and orbital periods. We find that the parameters α=1.5 and α=2 yield the best match to the theoretical value of this ratio (the ratio is one for a point mass potential).

The optimal selection of a power of 1.5 in radius appears to align with the orbital or radial period of the orbit. As per Kepler's third law, this period is proportional to $R^{3/2}$ where R denotes the semi-major axis of an elliptical orbit, thus supporting the use of this power. In other words, the time step with α=1.5 scales the local orbital period for a Keplerian orbit.

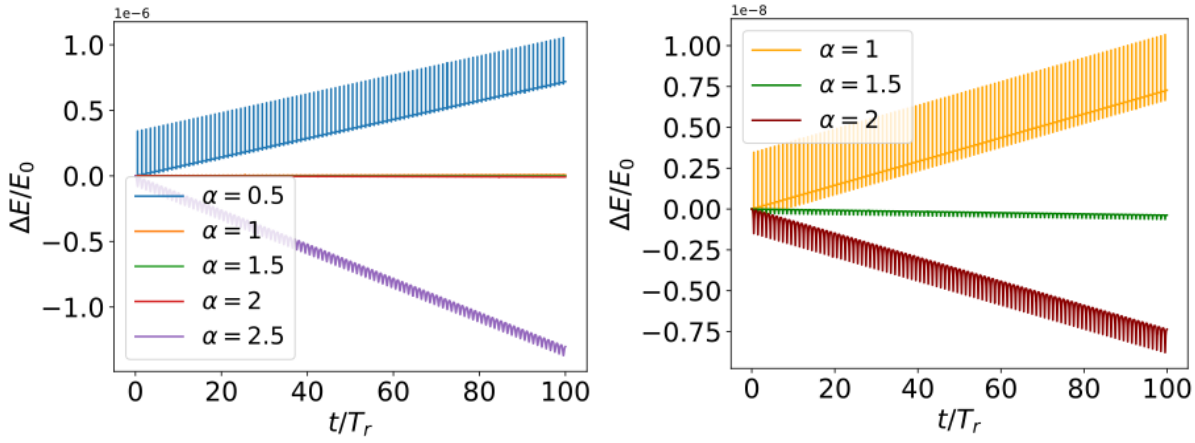

(a) (b)

Figure 3. The plot of the energy error drifts over 100 radial periods in the point mass potential (a) using α=0.5, 1.0, 1.5, 2.0, and 2.5, respectively. (b) using α=1.0, 1.5, 2.0, zoomed version to show apparent differences.

3.2 Application to Stellar Orbit at the Outskirts of a Globular Cluster

When a star resides on the outskirts of a globular cluster and orbits the cluster, the most straightforward potential to describe this scenario is the Plummer model, expressed as:

$$\Phi(r) = -\frac{GM}{\sqrt{r^2 + b^2}}, \tag{14}$$

where b is the scale radius.

This potential is considered a central potential, leading to the conservation of angular momentum. Consequently, as angular momentum remains constant, the star's orbit remains planar. The resulting orbit is a rosette, as depicted in Figure 4. This indicates that the numerical values of orbital and radial periods are different.

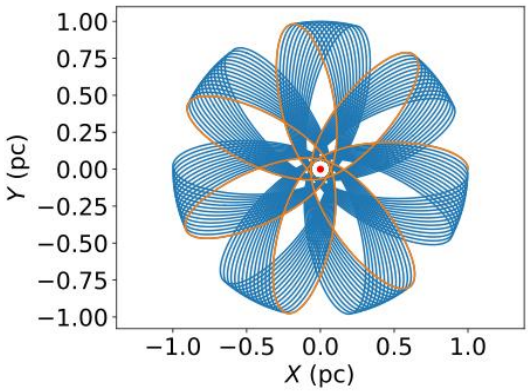

Figure 4. The orbit of a star in Plummer potential (GM = 1 and b = 0.1) with a time step of parameter α =1.5. The orange line represents the orbit for the first seven radial periods, while the blue line depicts the orbit for 100 radial periods.

For example, when we use GM=1 and b=0.1, the orbit completes one radial cycle, while the orbital cycle is only about 2/7 of the way through. In this case, the exact ratio of the orbital period to the radial period is irrational.

Our calculation of energy error exhibits a similar trend and identifies the most accurate power law (see Figure 5) as those observed in the point mass potential. Additionally, the phase space error can be significantly reduced with $\alpha = 1.5$ in our simulation.

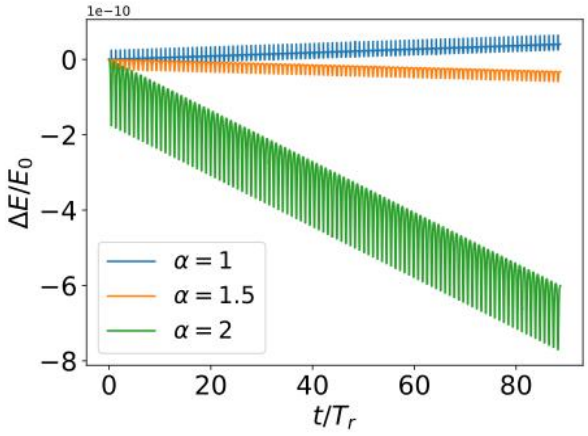

Figure 5. The plot of the energy error drifts within 100 radial periods in the Plummer potential using α=1.0, 1.5, and 2.0, respectively.

3.3 Application to Stellar Orbit at the Outskirts of a Globular Cluster

One of the simplest potentials for the distribution of stars in a spherical galaxy is the Hernquist potential, expressed as:

$$\Phi(r) = -\frac{GM}{r+b}. \tag{15}$$

where b is the scale radius. This potential is also appropriate for modelling the potential of a dark matter halo (Bovy, 2023).

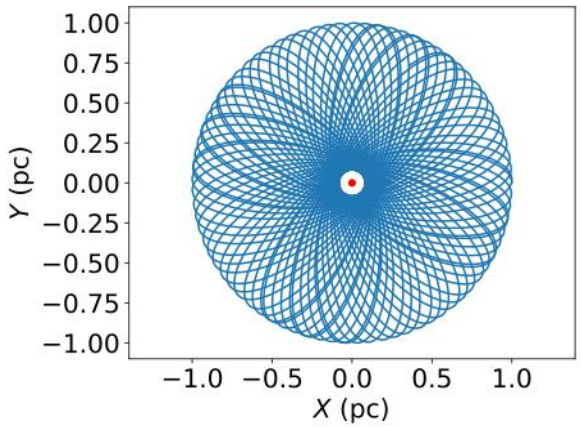

Figure 6. The eccentric orbit of a star in Hernquist potential (GM = 1 and b = 0.1) with a time step of α =1.5 for 100 radial periods. The ratio of the radial period to the orbital period is approximately 0.74.

The orbit of a star in this potential is a rosette, as depicted in Figure 6. This typical orbit is commonly found in the Hernquist potential (Adams & Bloch, 2005).

A similar trend in energy drift is observed in this potential, as shown in Figure 7. Once again, the simulation results with a time step power of α = 1.5 exhibited the minimum gradient of energy drift.

This outcome confirms that a power of 1.5 is optimal for various spherical potentials in the power law model of time steps.

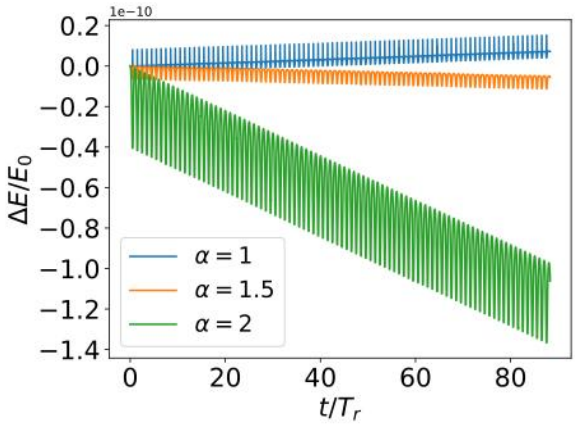

Figure 7. The plot of the energy error drifts over 100 radial periods in the Hernquist potential using α=1.0, 1.5, and 2.0, respectively.

4. CONCLUSION

We have developed and presented an algorithm for orbit integration in central conservative potentials, applied explicitly to point-mass, Plummer, and Hernquist models, by employing a power-law time step function. While the method has not yet been tested in more complex potentials, such as disk-like or galactic bulge configurations, our simulations across a range of exponents clearly demonstrate that orbital accuracy is maximised when the power-law index is set to 1.5. This choice directly corresponds to the radial period of orbital oscillation, consistent with Kepler's third law, and thereby provides a physically motivated basis for the timestep selection. The approach is both simple to implement and computationally efficient, making it well-suited for practical applications. Furthermore, the method has the potential to be extended to N-body problems or to more general dynamical systems beyond the cases tested here. Given its combination of theoretical grounding, numerical robustness, and ease of adoption, we expect this technique to be a valuable tool for enhancing orbit accuracy in a wide range of astrophysical contexts.

ACKNOWLEDGEMENT

Authors acknowledge support from DIPA Untan Fund Number DIPA-023.17.2.677517/2021, dated 17 November 2021, Fiscal Year 2022.

REFERENCE

Aarseth, S. J. (2003). Gravitational N-body simulations. In Gravitational N-Body Simulations, by Sverre J.~Aarseth, pp. 430. ISBN 0521432723.~Cambridge, UK: Cambridge University Press, November 2003. Cambridge University Press.

Aarseth, S. J., & Heggie, D. C. (1993). A 6000-body simulation with primordial binaries. In G. H. Smith & J. P. Brodie (Eds.), The Globular Cluster-Galaxy Connection (Vol. 48, p. 701).

Adams, F. C., & Bloch, A. M. (2005). Orbits in Extended Mass Distributions: General Results and the Spirographic Approximation. The Astrophysical Journal, 629(1), 204–218. https://doi.org/10.1086/431455

Baes, M., & Dejonghe, H. (2002). The Hernquist model revisited: Completely analytical anisotropic dynamical models. Astronomy and Astrophysics, 393(2), 485–497. https://doi.org/10.1051/0004-6361:20021064

Binney, J., & Tremaine, S. (2008). Galactic dynamics: Second edition. Princeton University Press.

Bovy, J. (2023). Dynamics and Astrophysics of Galaxies (in Preparation). Princeton University.

Chin, S. A., & Chen, C. R. (2005). Forward Symplectic Integrators for Solving Gravitational Few-Body Problems. Celestial Mechanics and Dynamical Astronomy, 91(3), 301–322. https://doi.org/10.1007/s10569-004-4622-z

Dehnen, W. (2017). Towards time symmetric N-body integration. Monthly Notices of the Royal Astronomical Society, 472(1), 1226–1238. https://doi.org/10.1093/MNRAS/STX1944

Dehnen, W., & Hernandez, D. M. (2017). Symplectic fourth-order maps for the collisional N-body problem. Monthly Notices of the Royal Astronomical Society, 465(1), 1201–1217. https://doi.org/10.1093/mnras/stw2758

Dehnen, W., & Read, J. I. (2011). N-body simulations of gravitational dynamics. European Physical Journal Plus, 126(5), 55. https://doi.org/10.1140/epjp/i2011-11055-3

Hands, T. O., Dehnen, W., Gration, A., Stadel, J., & Moore, B. (2019). The fate of planetesimal discs in young open clusters: implications for 1I/'Oumuamua, the Kuiper belt, the Oort cloud, and more. Monthly Notices of the Royal Astronomical Society, 490(1), 21–36. https://doi.org/10.1093/mnras/stz1069

Hasanuddin. (2020a). GitHub - hasanastro4/simpthon. Https://Github.Com/Hasanastro4/Simpthon.

Hasanuddin. (2022). Simulasi Orbit Planet Eksentrisitas Tinggi dengan Metode Leapfrog. Jurnal Fisika, 12(1), 1–8.

Hasanuddin, H. (2020b). Analisis Galat Energi dan Galat Fase Metode Forward 4th Order Symplectic Chin-Chen untuk Kasus Sistem Osilator Harmonik Sederhana. POSITRON, 10(2), 88–92. https://doi.org/10.26418/positron.v10i2.40023

Heggie, D., & Hut, P. (2003). The Gravitational Million-Body Problem: A Multidisciplinary Approach to Star Cluster Dynamics. In The Gravitational Million-Body Problem: A Multidisciplinary Approach to Star Cluster Dynamics, by Douglas Heggie and Piet Hut. Cambridge University Press, 2003, 372 pp.. Cambridge University Press.

Hernandez, D. M., & Dehnen, W. (2023). Switching integrators reversibly in the astrophysical N-body problem. Monthly Notices of the Royal Astronomical Society, 522(3), 4639–4648. https://doi.org/10.1093/mnras/stad657

Hernquist, L. (1990). An analytical model for spherical galaxies and bulges. Astrophysical Journal, 356, 359–364. https://doi.org/10.1086/168845

Leimkuhler, B., & Reich, S. (2005). Simulating Hamiltonian Dynamics (1st ed.). Cambridge University Press. https://doi.org/10.2277/0521772907

Pham, D., Rein, H., & Spiegel, D. S. (2024). A new timestep criterion for N-body simulations. The Open Journal of Astrophysics, 7, 1. https://doi.org/10.21105/astro.2401.02849

Plummer, H. ~C. (1911). On the problem of distribution in globular star clusters. Monthly Notices of the Royal Astronomical Society, 71, 460–470. https://doi.org/10.1093/mnras/71.5.460

Plummer, H. C. (1915). The Distribution of Stars in Globular Clusters. Monthly Notices of the Royal Astronomical Society, 76(2), 107–121. https://doi.org/10.1093/MNRAS/76.2.107

Zemp, M., Stadel, J., Moore, B., & Carollo, C. ~M. (2007). An optimum time-stepping scheme for N-body simulations. Monthly Notices of the Royal Astronomical Society, 376(1), 273–286. https://doi.org/10.1111/j.1365-2966.2007.11427.x

APPENDICES

Appendix A: Acceleration dan Tidal Force Tensor in Central Potential

When the central potential is formulated as shown below:

$$\Phi = \Phi(r), \tag{16}$$

as appear in equation (8) and (9), the acceleration corresponding to this potential is

$$a_i = -\frac{\partial}{\partial x_i}\Phi(r) = -\frac{x_i}{r}\frac{d\Phi(r)}{dr} \tag{17}$$

where index $i = 1, 2, 3$ and corresponding to the *x, y, and z* components in Cartesian coordinates, respectively. The tidal force tensor is

$$T_{ij} = \nabla(\nabla\phi) = \frac{\partial a_i}{\partial x_j} = -\frac{x_i x_j}{r^2}\frac{d^2\Phi(r)}{dr^2} + \left(\frac{x_i x_j}{r^2} - \delta_{ij}\right)\frac{1}{r}\frac{d\Phi(r)}{dr}. \quad (18)$$

where δ_{ij} is a function of Kronecker delta.

Appendix B: Acceleration dan Tidal Force Tensor in Point Mass Potential

Acceleration of a particle orbiting a point mass potential is

$$a_i = -\frac{GM}{r^3}x_i. \quad (19)$$

The corresponding tidal force tensor is

$$T_{ij} = \frac{GM}{r^3}\begin{pmatrix} 3\frac{x^2}{r^2} - 1 & 3\frac{xy}{r^2} & 3\frac{xz}{r^2} \\ 3\frac{xy}{r^2} & 3\frac{y^2}{r^2} - 1 & 3\frac{yz}{r^2} \\ 3\frac{xz}{r^2} & 3\frac{yz}{r^2} & 3\frac{z^2}{r^2} - 1 \end{pmatrix}. \quad (20)$$

Appendix C: Acceleration dan Tidal Force Tensor in Plummer Potential

The acceleration of a particle orbiting a Plummer potential is

$$a_i = -\frac{GM}{(r^2 + b^2)^{3/2}}x_i. \quad (21)$$

The corresponding tidal force tensor is

$$T_{ij} = \frac{GM}{(r^2 + b^2)^{\frac{3}{2}}}\begin{pmatrix} \frac{3x^2}{r^2 + b^2} - 1 & \frac{3xy}{r^2 + b^2} & \frac{3xz}{r^2 + b^2} \\ \frac{3xy}{r^2 + b^2} & \frac{3y^2}{r^2 + b^2} - 1 & \frac{3yz}{r^2 + b^2} \\ \frac{3xz}{r^2 + b^2} & \frac{3yz}{r^2 + b^2} & \frac{3z^2}{r^2 + b^2} - 1 \end{pmatrix}. \quad (22)$$

Appendix D: Acceleration dan Tidal Force Tensor in Hernquist Potential

Acceleration of a particle orbiting a Hernquist potential is

$$a_i = -\frac{GM}{r\,(r + b)^2}x_i. \quad (23)$$

The corresponding tidal force tensor is

$$T_{ij} = \frac{GM}{r(r + b)^2}\begin{pmatrix} \frac{(3r + b)x^2}{r^2(r + b)} - 1 & \frac{(3r + b)xy}{r^2(r + b)} & \frac{(3r + b)xz}{r^2(r + b)} \\ \frac{(3r + b)xy}{r^2(r + b)} & \frac{(3r + b)y^2}{r^2(r + b)} - 1 & \frac{(3r + b)yz}{r^2(r + b)} \\ \frac{(3r + b)xz}{r^2(r + b)} & \frac{(3r + b)yz}{r^2(r + b)} & \frac{(3r + b)z^2}{r^2(r + b)} - 1 \end{pmatrix}. \quad (24)$$